Soft Matter

Accepted Manuscript

ROYAL SOCIETY OF CHEMISTRY

www.rsc.org/softmatter

Journal Name

ARTICLE TYPE

Cite this: DOI: 10.1039/xxxxxxxxxx

Loss of Bottlebrush Stiffness due to Free Polymers†

Ingeborg M. Storm,*[a] Micha Kornreich,[b‡] Ilja K. Voets,[c], Roy Beck,[b], Renko de Vries,[a], Martien A. Cohen Stuart[a] and Frans A. M. Leermakers[a]

Received Date
Accepted Date

DOI: 10.1039/xxxxxxxxxx

www.rsc.org/journalname

A recently introduced DNA-bottlebrush system, which is formed by the co-assembly of DNA with a genetically engineered cationic polymer-like protein, is subjected to osmotic stress conditions. We measured the inter-DNA distances by X-ray scattering. Our co-assembled DNA-bottlebrush system is one of the few bottlebrushes known to date that shows liquid crystalline behaviour. The alignment of the DNA bottlebrushes was expected to increase with imposed pressure, but interestingly this did not always happen. Molecularly detailed self-consistent field calculations targeted to complement the experiments, focused on the role of molecular crowding on the induced persistence length l_p due to the side chains and the cross-sectional width D of the molecular bottlebrushes. Both the thickness as well as the backbone persistence length drop with increasing protein-polymer bulk concentrations and dramatic effects are found above the overlap threshold. The flexibilisation is more significant and therefore the bottlebrush aspect ratio, l_p/D, decreases with protein-polymer concentration. This loss in aspect ratio is yet another argument why molecular bottlebrushes rarely order in anisotropic phases and may explain why bottlebrushes are excellent lubricants.

1 Introduction

The term "bottlebrush" denotes macromolecular architectures that consist of a backbone with many densely attached and therefore stretched (compared to the Gaussian dimensions) side-chains.[1] Bottlebrush systems have been investigated intensively experimentally,[2–8] and from a theory[9–12] and simulations[13–19] perspective. A well known application for polymer brushes can be found in lubrication of materials.[20–24] The aggrecan molecule is a famous biological lubricant. Aggrecan is part of the articular cartilage that ensures the lubrication of joints in the human body.[25–28] This molecule in fact is a bottlebrush with side-chains that are bottlebrushes by themselves. Aggrecan has highly charged polysaccharide side chains and therefore has a tremendous capability to hold water even under large pressures. This ability to attract water results in a swollen structure that reduces the friction of the joints and thereby prevents wear.

Another biological bottlebrush system is the anisotropic neurofilament gel-like network which provides mechanical stability and strength to high aspect ratio neuronal cells. Neurofilaments have a compact rigid cylindrical core with polypeptide side-chains, which have an unstructured polymer-like projection domain that stretch away from the core due to electrostatic- and steric lateral interactions. The liquid crystalline network that neurofilaments form arguably have a role to resist external pressures.[29–33]

Recently we introduced a model bottlebrush system which is extremely well defined in molecular terms, but which is definitely less complicated than the natural counterparts and still features relevant physical properties such as the ability to order in liquid crystalline phases.[34] We use the semi-flexible double stranded DNA (dsDNA) chain as the core of the bottlebrush. For the side chains we use a recombinant protein polymer. The latter macromolecules are unique because they are strictly monodisperse and chirally pure. The name that is used, C_4K_{12}, reflects its functionality.[35] The binding block consist of 12 positively charged lysines (K_{12}) that bind electrostatically to the negatively charged DNA backbone. The C_4-block is a 400 aa hydrophilic randomly structured collagen-like block, a concatenation of four sequences of 100 aa (for the exact aa sequence see ref[35]). This collagen-like block has no significant secondary or tertiary structure and forms the corona of the DNA-protein polymer complex.[36] As the grafting density of the corona is sufficiently high, the thickness of the corona is more than twice the radius of gyration of the free protein, the C_4-chain blocks are strongly stretched.[34] That is why

[a] Physical Chemistry and Soft Matter, Wageningen University & Research, Stippeneng 4, 6708 WE Wageningen, The Netherlands. E-mail: frans.leermakers@wur.nl
[b] School of Physics and Astronomy, Tel Aviv University, Tel Aviv 69978, Israel.
[c] Laboratory of Macromolecular and Organic Chemistry, Laboratory of Physical Chemistry, and Institute for Complex Molecular Systems Eindhoven University of Technology Post Office Box 513, 5600 MD Eindhoven, The Netherlands.

† Electronic Supplementary Information (ESI) available: [Equilibration time of osmotic stress experiments and raw scattering data, I(q), are shown in ESI]. See DOI: 10.1039/b000000x/

we can refer to these complexes as co-assembled molecular DNA-bottlebrushes.

From a theoretical perspective we expect that co-assembled bottlebrushes can, to first order, be considered as supramolecular bottlebrushes with covalently grafted side chains. Fredrickson was the first to analyze the effect of side chains on the physical properties of the bottlebrush and hypothesized that the side chains would help flexible backbones (main-chains) to form liquid crystalline phases.[37] Subsequent self-consistent field modelling revealed that the induced persistence length increases quadratically with the coverage of side chains along the main-chain, i.e. $l_p \propto (N/h)^2$ where N is the number of segments of the side chains and h the distance between the side chains along the backbone, see Figure 1(a).[11] Theoretical approaches[11,38] agree that the thickness of a bottlebrush scales as $D \propto N^{3/4}h^{-1/4}$ and therefore one would expect the segment aspect ratio l_p/D to increase with increasing N and decreasing h. Although this behaviour is undisputed for large N, the very small value for the numerical prefactor for the mentioned persistence length l_p dependence, leads to the insight that in experimental cases the aspect ratio l_p/D remains small. Accordingly, it explains why most bottlebrushes are flexible and so few are known to form liquid crystals.

This does not imply that liquid crystallinity is excluded for bottlebrushes with a flexible backbone as exemplified by the synthetic liquid crystalline bottlebrush made by Wintermantel et al.[2] Their system is very similar to the ones reported by Tsukahara et al.[39] and Nakamura et al.[40] who report liquid crystallinity for a flexible backbone densely decorated by flexible polystyrene side chains. Another example of liquid crystallinity of bottlebrushes that have a flexible backbone is the PNIPAAM bottlebrushes of Li et al.[41] In this case the molecules align anisotropically when heated above the lower critical solution temperature (LCST). It appears the long side-chains collapse due to the fact that they become insoluble and thereby form anisotropically structured aggregates. The absence of sufficient examples in the past twenty years raises some questions regarding the feasibility of liquid crystals made from bottlebrushes with a flexible backbone. In the current paper we will argue that molecular crowding is yet another reason why bottlebrushes show a low tendency towards liquid crystallinity.

Bottlebrush molecules are critical components of systems which are required to withstand high external pressures.[42–45] To investigate how pressure influences the distances and alignment of our DNA-bottlebrushes we submitted the system to external osmotic pressures. We used large volumes of a poly(ethyleneglycol) (PEG) solutions[46,47], separated from the bottlebrush solution by a membrane to avoid the loss of protein C_4K_{12} chains. The inter-DNA spacing was measured by means of small angle X-ray scattering (SAXS) in the regime where the system is liquid crystalline. From the sharpness of the scattering peaks we extracted information on the alignment of the bottlebrushes. When most of the protein polymers was expected to be electrostatically bound to the DNA, the alignment improved with increasing pressure. However, when there was an excess of protein-polymer this was no longer the case. We concluded that molecular crowding has a negative impact on the propensity of bottlebrushes to form liquid crystalline phases.

Complementary self consistent field (SCF) calculations focused on the interaction between bottlebrushes in a cell model and extracted from this the osmotic pressure in the system as a function of the inter-chain distance. The same framework is used to predict how freely dispersed chains (molecular crowding) influences the induced persistence length and the cross-sectional diameter of molecular bottlebrushes. The latter calculations revealed that the segment aspect ratio goes down when the freely dispersed polymer concentration exceeds the overlap threshold. In line with our experiments, the SCF calculations thus indicate that molecular crowding inhibits liquid crystalline behaviour.

In our system the bottlebrushes are formed by a co-assembly of protein-polymers with dsDNA. In such a system the freely dispersed polymers cannot be ignored. As mentioned these freely dispersed polymers do affect the aspect ratio of the bottlebrush molecules. This observation is relevant for the biological context, as in biological systems bottlebrushes will never be in a single molecule state and invariably surrounded by freely dispersed macromolecules. The response of molecular bottlebrushes on such crowding molecules has been partly addressed in the literature. The reduction of the induced persistence length upon an increase in bottlebrush concentration was predicted in an early publication by Borisov et al.,[48] and experimentally shown by Rathgeber and Bolisetty,[49,50] but the effect of free polymer has not yet been explicitly considered.

2 Materials and methods

2.1 Production and purification of C_4K_{12}

The protein polymer used in this work, C_4K_{12}, was biosynthesized by genetically modified *Pichia Pastoris* cells, carrying a gene that encodes for the secreted expression of the diblock protein polymer C_4K_{12}.[35]

After the fermentation was completed the protein solution was separated from the yeast cells by centrifugation (16000 g, 30 min, 4 °C) and filtration (0.2 μm Acropak 200 capsules with Supor membrane from Pall Corporation). To purify the produced C_4K_{12} protein we first increased pH to 8 using NaOH and centrifuged (16000 g, 30 min, 4 °C) the protein solution to remove the majority of medium salts. After centrifugation C_4K_{12} proteins were separated from secreted *Pichia Pastoris* proteins by selective precipitation with ammonium sulphate (45% saturation). This precipitation step was performed for 30 minutes at 4°C. The C_4K_{12} pellet was redissolved in 0.2 times the original volume ($\sim$ 1 l) of 50 mM formic acid and extensively dialysed against 50 mM formic acid. During the last dialysis step the proteins were dialysed against a 10 mM formic acid solution. Consecutively, the C_4K_{12} solution was freeze dried.

2.2 DNA preparation

For the preparation of the DNA bottlebrushes we used DNA type II fibers (Sigma). The DNA was dissolved in a 10 mM Tris-HCl buffer of pH 7.6 to a concentration of 2 mg/ml. The DNA solution was sonicated with a Bandelin Sonopuls GM 70 (power 2/3 and

100% cycle) to decrease the length of DNA. The solution was sonicated for 10 minutes to obtain DNA fragments of approximately 500-1000 base pairs (bp).[34]

2.3 Sample preparation

The concentrated DNA-C_4K_{12} co-assemblies were prepared by mixing the DNA and C_4K_{12} in the desired ratio in a dilute solution. It was estimated earlier[34] that 10 g of protein is needed to completely neutralize 1 g of DNA. We therefore introduce the weight ratio $\Gamma = 10$ g/g and refer to this as the (charge) stoichiometric ratio. In our experiments we used this ratio and a three fold excess, i.e., $\Gamma = 30$ g/g.

After overnight incubation the samples were concentrated using centrifuge filters (Amicon Ultra-0.5 ml 3K membrane). The samples were washed with a 10 mM Tris-HCl buffer of pH 7.6 with 0.05% NaN_3 to remove excess salt. The DNA-C_4K_{12} complexes (typically 30 μl) were placed in small 3.500 MWCO Slide-A-Lyzer MINI dialysis units. These dialysis units were placed in a 40 ml solution, consisting of a specific PEG concentration. This PEG solution was made by first making a 40 wt% PEG solution in a 10 mM Tris-HCl buffer of pH 7.6 with 0.05% NaN_3. The 40 wt% PEG solution was then diluted with Tris buffer to the appropriate PEG concentration. The incubation period was one week. Conversion from wt% PEG to pressure was done according to:

$$\Pi = 10^{a+b\times(wt\%)^c} \quad (1)$$

where $a = 1.57$, $b = 2.75$ and $c = 0.21$.[46]

2.4 SAXS

Our concentrated samples were placed in Hilgenberg quartz capillaries with an outer diameter of 1 mm and a wall thickness of 0.01 mm. The concentrated samples for the osmotic stress experiments were measured on a SAXS-LAB instrument with a Xenocs GeniX Low Divergence Cu Kα X-ray source in combination with a Pilatus 300 K detector (Dectris, Baden, Switzerland). A wavelength of 1.54 Å was used together with sample-detector distances of 110, 710 and 1510 mm respectively. With these configurations we have a q-range available of 0.006-2.41 Å^{-1}. A typical data acquisition time was 1800 s. The 2D data was then radially averaged using the SAXSGUI software to produce 1D plots of intensity as a function of q.

The samples that consisted of a low concentration of DNA and protein polymers were used to determine the brush thickness of the DNA-bottlebrushes. For the samples we used 250 μg/ml λ-DNA in the presence of a three times excess amount of C_4K_{12} protein polymer of 7.5 mg/ml, which is denoted as $\Gamma = 30$. For the sample consisting only of free protein we used a concentration of 30 mg/ml. These low concentration samples were measured at the I911-4 beamline at MAXlab II, Lund, in Sweden. The q-range we used corresponded to 0.008-0.550 Å^{-1} with an incident wavelength of 1.2 Å. The samples were measured in a 'high throughput solution scattering set-up' to properly subtract the buffer from the sample at exactly the same location in the capillary. The detector used was a PILATUS 1M detector from Dectris. The acquisition time for each sample was 20 minutes. The data processing was done by using SASview 3.0.0 software.

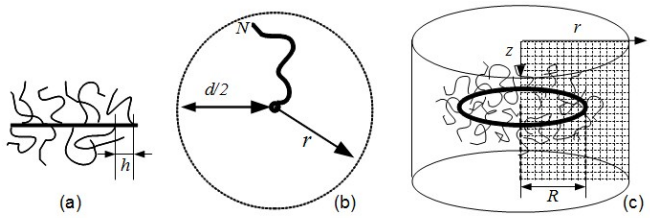

Fig. 1 A schematic bottlebrush molecule used in the SCF calculations where h is depicted as the distances between side chains (a). A top-view of a schematic representation of the cell model: where the backbone of the bottlebrush is in the middle of the figure going into the plane of the figure. The circular dotted line represents a mirror boundary condition, N the length of the side chains, $d/2$ is the distance between the brush and its image and r represents radial coordination (b). The third figure shows a two gradient cylindrical coordination system with a homogeneously curved bottlebrush. R is the radius of curvature (curvature is $J = 1/R$), z the direction along the longest axis of the cylinder and r the radial coordinate (c).

To fit our scattering data we used two types of models. To describe the experimental data collected for the free C_4K_{12} protein polymers in solution we used a model for polymers with excluded volume,[51,52] for the DNA-bottlebrushes we used a model for randomly oriented homogeneous cylinders.[53,54]

2.5 SCF-calculations

Numerical self-consistent field calculations with the discretisation scheme of Scheutjens and Fleer (SF-SCF)[55] have been performed using the sfbox program. In this approach the volume is represented by a lattice with characteristic size $b = 5 \times 10^{-10}$ m. All linear lengths are given in units b. Macromolecules are modeled as freely jointed chains (FJC) with segment size equal to the lattice site. In the FJC model two consecutive bonds along the chain have uncorrelated directions, while nearest neighbor segments occupy nearest neighbor lattice sites. In contrast to Gaussian chains, FJC thus have a finite extensibility. Below we will use a one-gradient cylindrical coordinate system (cell model) to evaluate the pressure-distance relation for compressed bottlebrushes (cf. Figure 1(b)). In this case we have cylindrically curved layers of lattice sites $\mathbf{r} = r = 1,\ 2,\ \cdots\ d/2$, where d is the distance between two DNA chains. The number of lattice sites at r is given by $L(r) = 2r - 1$. A two-gradient cylindrical coordinate system is used to evaluate the induced persistence length (cf. Figure 1(c)). In this case we have coordinates $\mathbf{r} = (z, r)$, where the radial coordinate is similar to the one-gradient case and the z-coordinate is used to number lattice layers in the direction along the cylinder axis $z = 1,\ , 2 \cdots ,\ M$.

Typical for the SCF theory a local mean-field approximation is introduced, which means that at a given coordinate $\mathbf{r}$ the segment densities are averaged, so that the relevant concentration can be expressed as a volume fraction $\varphi(\mathbf{r})$. Using this mean-field approximation it is possible to enumerate the number of contacts between segments in the system and each contact is weighted by the Flory-Huggins interaction parameters, which are non-zero

for all unlike contacts. The SCF theory is based on optimization of a free energy functional, which leads to a SCF "machinery" working as follows. The effect of surrounding molecules on the conformation of a particular component X is expressed in terms of a potential field $u_x(\mathbf{r})$ which is computed from the volume fractions $\varphi_X(\mathbf{r})$ of the segments. The volume fractions, in turn, can be found after statistical evaluation of the conformations.

2.5.1 Osmotic stress calculations.

Osmotic stress calculations are performed in a one-gradient cylindrical coordinate system. A graphical representation is given in Figure 1(b). The DNA chain is assumed to sit with its center-of-mass at $r = 0$. The bottlebrush is composed of N segments of which the first segment is constrained to be at the DNA main-chain location. For each calculation the number of chains per unit length $(1/h)$ of the DNA is an input quantity.

For a given SCF solution we have the free energy of the system available. The free energy can be expressed in terms of the volume fraction and segment potential profiles $F = F(\{\varphi, u\})$ [55]. In the cell model we can compute the free energy for a given value of the cell size $d/2$. At the system boundary we have reflecting boundary conditions which implies that the 6 'images' (assuming hexagonal ordering) of the central DNA chain are located at a distance d from the central chain. After the SCF equations are solved the free energy is recorded as $F(d/2)$. Subsequent variations of the value of d give a free energy interaction

$$\Delta F(d/2) = F(d/2) - F(\infty) \tag{2}$$

where the reference $F(\infty)$ implies that we are interested in an excess pressure and the free energy is given in lattice units of $k_{\mathrm{B}}T/b$ wherein b is the segment length. To obtain a pressure we first need to go to a free energy per unit area. That is why the free energy is divided by the length of the circumference of the upper boundary

$$\Delta f(d/2) = \frac{\Delta F(d/2)}{\pi d} \tag{3}$$

Now the osmotic pressure is found by differentiation, i.e. $\Pi = -\partial f/\partial d$. This is implemented on the lattice by taking a difference between two cell sizes:

$$\Pi(d/2) = -2\left(f(d/2) - f(d/2-1)\right) \tag{4}$$

where the factor of 2 is needed because a change in the cell size by one implies a distance d change of two. The pressure is given in units $k_{\mathrm{B}}T/b^3$. Using a lattice size $b = 5 \times 10^{-10}$ m, gives for $\Pi(d) = 1$ a pressure of 32×10^6 Pa.

2.5.2 Induced persistence length.

Referring to Figure 1(c) for an illustration, we position a bottlebrush chain with its backbone location $\mathbf{r} = (M/2, R)$ such that the radius of curvature is R and the curvature of the backbone is $J = 1/R$. Onto the backbone we pin linear chains with length N by their first segment. The contour length of the torus-like backbone is $L = \pi(2R-1)$ and thus we fix the number of chains to the backbone to be $n = L/h$. The mean-field approximation allows for non-integer number of grafted chains. In the calculations we allow for freely floating PEG polymers in solution. As the volume fraction of these chains is an input quantity, we compute the characteristic free energy of the system as

$$\Omega(J) = F(J) - n_{C_4}\mu_{C_4} - n_S\mu_S \tag{5}$$

μ_{C_4} and μ_S is the chemical potential of the protein-polymers and solvent respectively (unique function of the volume fraction in the bulk), and n_{C_4} is the number of C_4 (free-floating) chains in the system. As J is a small quantity with respect to the uncurved bottlebrush, we can expand in a Taylor series the free energy per unit length $\omega = \Omega/L$:

$$\omega(J) = \omega(0) + \frac{1}{2}k_{\mathrm{c}}J^2 \tag{6}$$

Here $k_c = \frac{\partial^2\omega}{\partial J^2}$ is the bending rigidity which has the units k_BTl. The odd terms in J can be omitted for symmetry reasons and higher order terms are omitted as we will consider only the limit of small values of J. Dividing the bending rigidity by the thermal energy may be identified as the induced persistence length

$$l_{\mathrm{p}} = \frac{k_{\mathrm{c}}}{k_{\mathrm{B}}T} \tag{7}$$

It is easily checked that bending a chain with length $2l_{\mathrm{p}}$ with a curvature given by $J = 1/l_{\mathrm{p}}$ will deflect the chain by about 60 degrees from its original direction.

In practice we evaluate $\omega(J)$ for a series of J values and then plot $(\omega(J) - \omega(0)) \times 2/J^2$ as a function of J. The idea is that a horizontal line will result, which lies at k_{c}. Important for this procedure is an accurate value of $\omega(0)$. As lattice artifacts introduce numerical noise in the calculations, we fine tune the value of $\omega(0)$ such that the predictions of k_{c} are evenly distributed around an average value, which is then taken as the final results.

2.5.3 Bottlebrush cross-sectional diameter.

In this section we examine the cross-sectional radius of the bottlebrush. We compute this in the cell model with freely dispersed C_4 chains in solution. The radial volume fraction profile for the grafted chains is directly available after the SCF equations have been solved. We use the first moment of the distribution of the end-segments of the grafted chains to estimate the extension (height) of the bottlebrush:

$$D = \frac{1}{h}\sum_r r \cdot n(r) \tag{8}$$

Where $n(r) = \pi(2r-1)\varphi_e(r)$ is the number of end-points located at a distance r (in lattice units) from the central DNA chain. The factor $1/h$ equals the number of (side) chains per unit length along the DNA main-chain.

2.6 Modelling parameters

As mentioned before, all linear lengths are presented in lattice units b, for which we take $b = 5 \times 10^{-10}$ m. In the experiments we have C_4K_{12} chains of which the 12 lysines represents the binding domain. We do not cover here the physisorption mechanism and represent the bottlebrush by covalently linked chains onto a rigid phantom backbone. Freely dispersed polymers are therefore also

taken to have 400 segments. In theoretical studies one typically chooses athermal solvent conditions. However, as we are aiming the calculations to represent the experimental case, we consider a 'marginal' solvent having a more realistic (still ad hoc) value $\chi = 0.4$, typical for many water-soluble polymers. The distance between chains in the bottlebrush is estimated from previously measured binding isotherms to be around 2 nm which implies $h \approx 4$.[34] We have varied h around this estimated value and used $h = 2$, 4, and 8.

3 Results and discussion

In this section we will first discuss X-ray scattering experiments on dilute samples from which we extract the bottlebrush structure in the presence of freely dispersed protein-polymers. In the analysis of the osmotic stress experiments we focus on the position and the width of the first structure peak. The SCF calculations are presented in the second half of this section.

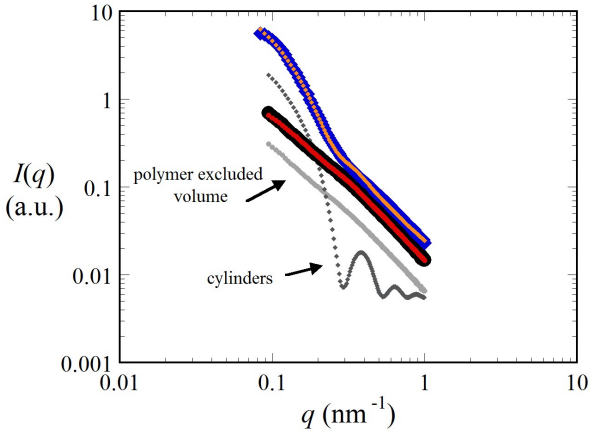

Fig. 2 Small angle X-ray scattering $I(q)$ curves of (i) the DNA-C_4K_{12} complexes (250 μg/ml of DNA) (blue) in the presence of excess protein polymers ($\Gamma = 30$) and (ii) C_4K_{12} protein solution (10 mg/ml) (black) with corresponding fittings as discussed in the text. The gray curves represent the relative contributions to the fit of the total scattering curve. For clarity reasons, the relative contributions were scaled down.

3.1 Thickness of Brush Layer

In principle one can extract the structural information of the molecular bottlebrushes from small angle X-ray scattering. These experiments are challenging because the data have to be taken at concentrations low enough to ignore the structure factor, implying long acquisition times. Fortunately, the structure factor information can be pushed to lower values of q such that it is possible to extract the cross-sectional information from the X-ray scattering from the $0.1 < q < 2$ nm^{-1} range, cf. in Figure 2. In this example we have besides the DNA-bottlebrush also freely dispersed protein polymers. That is why the fitting is still non-trivial.

Let us first focus on the scattering of freely dispersed protein polymers C_4K_{12} also shown in Figure 2 (in black). In this case the free protein-polymer has a concentration of 10 mg/ml and is dissolved in a 10 mM Tris-HCl buffer of pH 7.6. These molecules behave polymer like and that is why we used a "polymer excluded volume" model. The corresponding fit (red) gives a radius of gyration of 8.3 nm for the protein polymer C_4K_{12} which is reasonable for a polymer consisting of 400 segments.

The DNA-bottlebrushes in the presence of free protein produce the blue scattering profile in Figure 2. The data was fitted by a model combining two scattering entities: (i) a cylinder and (ii) a polymer with excluded volume. The fitting parameters for the polymer excluded volume model were taken from the reference sample of free C_4K_{12} protein polymer. The information for the brush diameter can be obtained from the q-range: $0.1 < q < 0.3$ nm^{-1} where the scattering from the bottlebrush dominates over the scattering of the free protein. As a brush radius we find 13 nm, which is about twice the radius of gyration of the free protein. This means that the side-chains were forced to stretch when attached to the DNA backbone molecule. This is in line with previously reported binding isotherms[34] from which it was estimated that under the present conditions there is about one C_4K_{12} chain per 2.7 nm DNA contour length, which implies short grafting distances. Much closer than the R_g value of 8.3 nm for the free protein.

3.2 Osmotic Stress Experiments

The driving force for bottlebrush formation is the attraction of opposite charges. More specifically, the positive charges of the lysines tend to form ion pairs with the negative phosphate charges on the DNA thereby releasing the counterions. The binding strength of this interaction is expected to decrease with increasing salt concentration. Here and below we used an ionic strength of 10 mM. With an increasing amount of protein polymers in the system we expect an increased binding. However, with increased coverage the C_4 tails becomes concentrated and progressively become stretched and this gives a counter force for adsorption. In addition, the net negative charge on the complex decreases with coverage. Hence the driving force for adsorption decreases with increasing coverage. For this reason it is not expected that full coverage is found at $\Gamma = 10$ g/g, and it can not be avoided that some of the protein molecules must remain in solution. In our previous paper[34] we estimated that the coverage under these conditions is close to 75%. The choice to also perform experiments for the ratio $\Gamma = 30$ g/g is motivated by the wish to increase the coverage to values closer to unity. However, at this ratio, at least two out of three of the protein polymers will remain unbound and disperse in the solution. When an osmotic pressure is applied to such a solution, the volume available for the freely dispersed polymers is little and the concentration of polymer consequently will be in the semi-dilute regime.

In previous experiments[34] we concentrated DNA-protein-polymer complexes by centrifugation and then changed concentration by dilution. In such experiments it is unknown at what osmotic pressures the resulting complexes reside. Therefore we performed osmotic stress experiments. The liquid crystallinity of our samples facilitated the measurement of the inter-DNA distances by X-ray scattering. We performed the osmotic stress experiments by bringing the DNA protein-polymer solution in contact with a PEG solution. We first tried to do this without using a membrane.

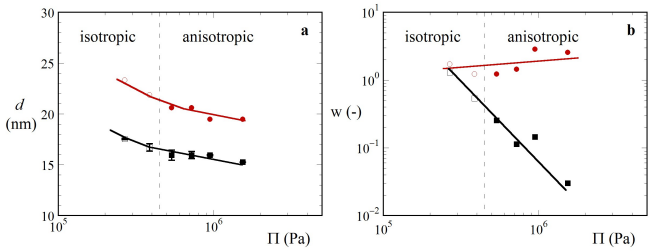

Fig. 3 a) The distances, d (nm), estimated from the position of the first Bragg peak between DNA-bottlebrushes as a function of the osmotic pressure Π (Pa) in lin-log coordinates. b) The corresponding dimensionless width w as a function of the pressure Π (Pa) in log-log coordinates. The red data points represent samples with a protein to DNA charge ratio of $\Gamma = 30$ and the black data points have a ratio of $\Gamma = 10$. Closed symbols belong to anisotropic samples, open symbols correspond to isotropic samples and a vertical dashed line is used to demarcate the isotropic- from the anisotropic phase.

It was found that the PEG solution phase separated from the DNA-bottlebrush solution, but that individual protein polymers slowly diffused into the PEG phase. Over time the protein-polymers detached from the DNA, which was concluded from a drift in the inter-DNA spacing. For this reason a membrane was used which prevented the protein-polymers from leaving the system and also prevented the PEG solution from entering the system. The equilibration time of the osmotic stress experiments is faster than one day as proven by the time evolution of the position of the first Bragg-peak shown in Figure 1 of the ESI†. To be on the safe side we, therefore, equilibrated our samples for one week prior to SAXS measurements.

The inter-DNA distances d are found from the positions of the first Bragg-peaks of the X-ray scattering curves. To find precise peak positions, we fitted $I(q) \times q$ by a parabola: $I = I(q_0) + b_q(q - q_0)^2$ in a q-range near the first Bragg peak. From this fit we found the position of the maximum q_0, and the corresponding distance d follows from

$$d = \frac{2\pi}{q_0} \qquad [\text{nm}] \tag{9}$$

whereas the width of the peak is made dimensionless by

$$w = b_q q_0^2 \tag{10}$$

The resulting distances d are presented in Figure 3(a) as a function of the osmotic pressure of the PEG solution (the corresponding scattering data $I(q)$ for both $\Gamma = 10$ and $\Gamma = 30$ can be found in Figure 4 and 5 respectively). In Figure 3(b) we give the corresponding dimensionless width of the first Bragg peak.

Figure 3(a) shows that, for given values of the osmotic pressure, the sample with the excess amounts of protein polymer ($\Gamma = 30$) has about 5 nm larger distances between the DNA backbone of two adjacent DNA-bottlebrushes than that at stoichiometric composition ($\Gamma = 10$). Recall that the typical size of the brush has a diameter of 26 nm. Hence when the inter-DNA distance is less than 26 nm the brushes are confined by the applied osmotic stress. Inspection of Figure 3(a) shows that in the range of applied pressures all distances are significant less than the unperturbed diameter, and we conclude that the brushes are compressed, to a maximum extent of about a factor of two.

To a reasonable approximation the distance between the bottlebrushes is a logarithmic function of the osmotic pressure. The weak curvature indicates the pressure increases somewhat more than exponential with decreasing distance. Upon reducing the distance between the bottlebrushes one will always concentrate the proteins because they can not escape from the system. In the modelling (see below), such concentration effect is not accounted for.

In passing we mention that at very low applied pressures ($\Pi < 4 \times 10^5$ Pa) the anisotropy of the solution was lost as judged from illumination through a crossed-polarizer set-up. The points for which this was the case are given by the open symbols, whereas all the anisotropic solutions are represented by closed symbols in Figure 3. Note that no jump in distances is observed at the pressure where the anisotropy of the solution is lost, indicating that the density differences between the isotropic and anisotropic phases is minute. The higher order scattering observed in the Figures 4 and 5 demonstrates that the anisotropic phase corresponds to a hexagonal liquid crystalline phase which we discussed in more detail previously.[34] The relative hexagonal peak positions of; 1, $\sqrt{3}$, $\sqrt{4}$, and if present, $\sqrt{7}$ are indicated in the scattering curves of Figure 4 and 5.

One might expect that with increasing applied osmotic pressure the bottlebrushes are pushed against each other and therefore would become more perfectly ordered. One thus would expect the first Bragg peak to sharpen up upon an increase of the osmotic pressure. Upon comparing the scattering curves of $\Gamma = 10$ with $\Gamma = 30$ (Figure 4 and 5) it can be seen that the Bragg peaks of $\Gamma = 10$ indeed become sharper and more pronounced, but the peaks of the $\Gamma = 30$ samples do not. So the expected increase in order upon the increase of the osmotic pressure is seen for $\Gamma = 10$ but not for $\Gamma = 30$ samples.

The measured width of the first Bragg peaks is shown in Figure 3(b). Inspection of this figure proves that the width decreases (as a power-law) for the stoichiometric case $\Gamma = 10$, whereas it is almost constant or becomes even wider with pressure for the protein overdosed system, $\Gamma = 30$. At this stage we may speculate about why the ordering for the $\Gamma = 30$ samples does not increase. The first explanation that comes to mind is that the excess of protein-polymer takes up so much space that the alignment of the liquid crystal is simply disrupted. As mentioned earlier, the excess proteins cannot escape the system and should therefore still be present in quite large quantities. Neither by using SAXS nor a crossed-polarizer set-up could we find any indication that the bottlebrushes and the free polymers are macroscopically separated from one another. Our C_4K_{12} protein polymers are also not known to interact attractively with C_4K_{12} free polymers[35] so C_4K_{12}-C_4K_{12} binding instead of DNA-C_4K_{12} interactions are highly unlikely. In such case there are only two options left for the freely dispersed chains: (i) they disperse through the brush or (ii) they reduce the brush height in order to generate space for themselves. Below we will return to this issue and present arguments in favour of the latter, because this mode can explain the loss in liquid crys-

talline ordering of our DNA-C_4K_{12} bottlebrushes.

3.3 Self Consistent Field Calculations

We use SCF theory to model molecular bottlebrush structure and thermodynamics (mechanics) with the aim to find possible explanations for these rather surprising results. We decided not to consider the electrostatic binding adsorption mechanism and opted for a bottlebrush model for which the grafting density is an input quantity ($h = 4$ is the default and $h = 2$, 8 are used for comparison reasons). We have seen that, experimentally, there is an effect of freely dispersed polymer and that is why we keep the bulk concentration of polymer as an extra control parameter in the calculations. A bulk volume fraction of $\varphi^b \approx 0.01$ signals the start of the overlap (semi dilute) regime. We stress that in experiments the polymer concentration and the grafting density are coupled parameters. Not so in our model for which we can treat these parameters as independent.

Let us first focus on the SCF prediction of the cross-sectional distribution of the side chains. In Figure 6 we present the radial volume fraction distribution of the grafted side chains. Wijmans *et al.* have shown that in the first few layers a power-law decay is found which gives way to a quasi-parabolic profile in the outer region of the profile.[56] Completely in line with this the radial concentration profile drops quickly with increasing distance from the main-chain (increasing r). When free polymer is added to the system we notice a significant compression. Clearly, as soon as the concentration of polymer exceeds the local density in the brush, it becomes favorable for the brush chains to reduce the tension along the chain and become more dense. Below we will quantify this effect. In the inset of Figure 6 we present the distribution of the free ends. This distribution is bell-shaped: the ends can distribute throughout the brush albeit that they tend to avoid the region extremely close to the backbone. The average position of the ends is taken as a measure of the brush size and is indicated by the vertical dotted lines.

The brush dimension D is computed for three values of h (2, 4, and 8) as a function of the bulk volume fraction of freely dispersed polymers and presented in lin-log coordinates in Figure 7. Obviously the brush height increases with increasing grafting density (decreasing h) closely following the theoretical power-law prediction $D \propto h^{-1/4}$ (not shown). With respect to the dependence on the polymer concentration in the bulk, there are clearly two regimes. As long as the polymer concentration in the bulk remains dilute the brush height is independent of the polymer concentration. For higher concentrations the height drops steeply (approximately logarithmic) with the bulk volume fraction.

The compression of the brush by free polymers may also be seen as a compression due to an applied osmotic stress. In this case the stress is due to the concentration of the polymers. In the semi-dilute regime the mean-field pressure of a polymer solution is expected to scale quadratically with the polymer concentration. Hence the almost linear drop with $\log(\varphi^b)$ implies a corresponding drop with applied $\log(\Pi)$. One may argue that there is a difference between compressing the brush with an opposing brush or with freely dispersed polymers. However these differences are minor especially as the dominant factor is driven by the polymers avoidance from interpenetration.

Before presenting the results of the cell-model we will first briefly present our results of the induced persistence length of the bottlebrush as a function of the bulk volume fraction of freely dispersed polymers ($\varphi^b_{C_4}$). To the best of our knowledge there are no predictions in the literature for this dependence. In Figure 8 we show the results in double logarithmic coordinates for three values of the grafting density. Analytical theory predicts that the induced persistence length increases quadratically with $1/h$ and the calculations are in good agreement with this.[11,38] As in Figure 7, which depicts D vs. $\varphi^b_{C_4}$, we again see two regimes. For concentrations below overlap the bending rigidity of the bottlebrushes is independent of $\varphi^b_{C_4}$. However, above this concentration there is a power-law dependence with a slope not far from -1. Hence the induced persistence length drops inverse proportionally to the bulk volume fraction of freely dispersed polymers as soon as the bulk concentration of polymers is in the semi-dilute regime. Apparently, as soon as the brush chains are no longer strongly stretched, the bottlebrush loses most of its induced rigidity.

As explained above, within a cell model we can confine a central bottlebrush by a homogeneously distributed set of neighboring bottlebrushes. The primary result is an increase of the free energy of the system with decreasing spacing d between the chains. Here we do not present such 'interaction' curves. Instead we focus on the distance between the bottlebrushes as a function of the (computed) osmotic pressure. The result is given in Figure 9 for three values of the grafting density and in the absence of freely dispersed polymers. These predictions should be compared to the experimental results given in Figure 3. Quite obviously the distance is a decreasing function of the osmotic pressure. On the lin-log scale we find, in accordance with the experimental data, roughly a straight line and the slope is consistent with experiments as it decreases somewhat with coverage. The slight curvature in $d(\log\Pi)$ indicate that the pressure is increasing slightly stronger than exponential with decreasing distance, again in accordance with the experimental data. Clearly, with increasing grafting density (reduction of h) for given pressure the distances are larger when the grafting density is higher (h smaller); the explanation for this is analogous to that given for D versus φ^b.

4 Discussion

In this paper we have presented osmotic stress experiments of DNA-bottlebrushes formed by the attraction of positively charged C_4K_{12} protein polymers to negatively charged DNA and compared the results to self-consistent field predictions. We found semi quantitative agreement for the compression curves $d(\Pi)$.

In the absence of free polymers, SCF results showed slightly superlinear behaviour of $d(\log\Pi)$. In complementary calculations wherein we fixed the amount of free polymer at a given initial distance between the bottlebrushes and then reduced the distance between the bottlebrushes, we also found slightly stronger than linear scaling of D with $\log\Pi$. We do not present these results in more detail here, because the results depend strongly on the initial distance at which the interaction curves were taken. Even

though experimentally a similar problem may exist we decided not to further elaborate on this.

We argued above that there is a close analogy between compressing a polymer brush by increasing the free polymer concentration and by reducing the distance between two bottlebrushes. In the latter case the height of the brush is pushed back with the help of a similar brush whereas in the former case this is done by a semi-dilute solution of isotropic chains. The backbone of the bottlebrush feels its side chains only when these are stretched and then there is an induced contribution to the persistence length. When compressed, e.g. by freely dispersed polymers or by nearby bottlebrushes (in the osmotic stress experiments) the side chains are no longer strongly stretched and thus the main chain does no longer notice its side chains and the persistence length approaches that of the backbone.

In analyzing the osmotic stress experiments it was noticed that the alignment of the DNA bottlebrushes with increased osmotic stress did only occur in the system for which the free polymer concentration was low. In the case where the protein-polymer concentration was relatively high, it was found that the brush height increased, however the alignment of the DNA bottlebrushes failed to go up, as proven by the insensitivity of the peak width of the first Bragg-peak in the X-ray scattering curves with increased osmotic pressure. The SCF results theory indicates that the height of the brush increases with decreasing h. Hence the experimentally found increase in the brush height for larger values of Γ may be explained by an increased coverage. SCF calculations further showed that an increase of the concentration of free polymer, especially above the overlap concentration, will cause a drop of the brush height. The free polymers compress the brush. We note that this reduction of the brush height is also visible experimentally when the diameter of the dilute bottlebrushes (extracted from Figure 2) is compared with the diameter of the compressed bottlebrushes (Figure 3a). Again, as mentioned already the modeling results proved that the induced persistence length dropped with increasing free polymer concentration. In Figure 10 we present the corresponding predictions for the aspect ratio l_p/D as a function of the free polymer concentration for three values of the grafting density. As expected the aspect ratio is independent of the polymer concentration in the dilute regime. However, the aspect ratio drops sharply with polymer concentration in the semi-dilute regime. This drop is caused by the fact that the induced persistence length is much more affected than the brush height when the polymer concentration is increased. Clearly, the free polymer concentration induces a flexibilisation of the bottlebrush in the semi-dilute regime. This flexibilisation has a negative influence on the alignment of the DNA bottlebrushes.

The use of side chains in a supramolecular bottlebrush architecture was thought to be a generic way to turn a flexible backbone into a semi-flexible macromolecule which would upon increasing concentration go to a liquid-crystalline ordering.[37] Yet, it rarely happens; our case of co-assembled DNA bottlebrushes is a rare example of supramolecular bottlebrushes that do show such anisotropic ordering. We now understand that by increasing the polymer concentration, the compression of the bottlebrushes leads to a reduction of the stretching of the side chains. This in turn reduces the induced persistence length. This reduction by freely dispersed polymer is believed to be analogues to the reduction upon increasing bottlebrush concentration which is already discussed in literature.[48–50] As a result of this, the induced persistence length decreases sharply with increase of free polymer concentration or with increase of the bottlebrush concentration. In other words, at high concentrations of the bottlebrushes it is the bare persistence length of the backbone that counts; in our experimental case the bare chain is DNA, which is semi-flexible with a significant persistence length of 50 nm. Hence this system can maintain its ordering upon compression. However, a bottlebrush made of a flexible backbone may not show similar behaviour and will randomise its directions upon concentrating the solution. We therefore arrive at the conclusion that orientational order of molecular bottlebrushes is more favourable for semi-flexible backbone chains.

In the introduction it was elaborated that bottlebrush molecules are interesting candidates for lubrication applications and biological examples are available. We may now speculate that for good lubrication properties the system should resist a compression induced crystallization, because this would have negative impact on lubrication. Bottlebrushes have the property that the molecules become more flexible upon compression and thereby potentially keep performing as a lubricant under pressure. At the same time the bottlebrushes are rather stiff in the absence of external forces which may help to maintain a baseline viscosity in the system.

5 Conclusion

We investigated the effect of free polymers and externally induced osmotic pressure using X-ray and SCF calculations on liquid crystalline co-assembled DNA-bottlebrushes. The co-assembly was formed by attraction of a positively charged protein polymer to a negatively charged semi-flexible DNA backbone. We compared experiments to self-consistent field calculations using a molecularly realistic model. We find semi quantitative agreements between theory and experiment. The mean separation between the bottlebrushes decreases close to logarithmically with imposed pressure. We find that with increasing pressure the alignment of the DNA bottlebrushes only occurred when there was a low concentration of freely dispersed protein polymers in solution. We argue that freely dispersed polymers have a negative effect on the aspect ratio of the bottlebrush polymers. When the free polymer concentration is in the semi-dilute regime, it compresses the bottlebrush side chains. This implies a reduction of the stretching of the side chains which in turn sharply reduces the induced persistence length: the flexibility of the bottlebrush reduces to that of the backbone. Our results may explain why in practice it is necessary to start with a semi-flexible backbone chain in order to come up with molecular bottlebrushes that feature liquid crystalline ordering. This conclusion is relevant for practical applications of bottlebrushes and their implication for the understanding of biological relevant bottlebrush systems. The flexibilisation of bottlebrushes under compression may explain why bottlebrushes are excellent lubrication additives.

Acknowledgement

This work was financially supported by a European Research Council Advanced Grant (Biomate, ERC-267254).

References

1 S. T. Milner, *Science*, 1991, **251**, 905–914.
2 M. Wintermantel, K. Fischer, M. Gerle, R. Ries, M. Schmidt, K. Kajiwara, H. Urakawa and I. Wataoka, *Angew. Chem. Int. Ed.*, 1995, **34**, 1472–1474.
3 M. Wintermantel, M. Gerle, K. Fischer, M. Schmidt, I. Wataoka, H. Urakawa, K. Kajiwara and Y. Tsukahara, *Macromolecules*, 1996, **29**, 978–983.
4 O. Ikkala, J. Ruokolainen, G. ten Brinke, M. Torkkeli and R. Serimaa, *Macromolecules*, 1995, **28**, 7088–7094.
5 K. Terao, T. Hokajo, Y. Nakamura and T. Norisuye, *Macromolecules*, 1999, **32**, 3690–3694.
6 H. Iwawaki, O. Urakawa, T. Inoue and Y. Nakamura, *Macromolecules*, 2012, **45**, 4801–4808.
7 Y. Hatanaka and Y. Nakamura, *Polymer*, 2013, **54**, 1538 – 1542.
8 K. Inoue, S. Yamamoto and Y. Nakamura, *Macromolecules*, 2013, **46**, 8664–8670.
9 T. M. Birshtein, O. V. Borisov, Y. B. Zhulina, A. R. Khokhlov and T. A. Yurasova, *Polym. Sci. U.S.S.R.*, 1987, **29**, 1293 – 1300.
10 A. Subbotin, M. Saariaho, R. Stepanyan, O. Ikkala and G. ten Brinke, *Macromolecules*, 2000, **33**, 6168–6173.
11 L. Feuz, F. A. M. Leermakers, M. Textor and O. V. Borisov, *Macromolecules*, 2005, **38**, 8891–8901.
12 A. Subbotin, M. Saariaho, O. Ikkala and G. ten Brinke, *Macromolecules*, 2000, **33**, 3447–3452.
13 M. Saariaho, I. Szleifer, O. Ikkala and G. ten Brinke, *Macromol. Theory Simul.*, 1998, **7**, 211–216.
14 M. Saariaho, O. Ikkala, I. Szleifer, I. Erukhimovichm and G. ten Brinke, *J. Chem. Phys.*, 1997, **107**, 3267–3276.
15 A. A. Darinskii, I. M. Neelov, A. Zarembo, N. K. Balabaev, F. Sundholm and K. Binder, *Macromol. Symp.*, 2003, **191**, 191–200.
16 P. E. Theodorakis, H.-P. Hsu, W. Paul and K. Binder, *J. Chem. Phys.*, 2011, **135**, 164903–1–12.
17 H.-P. Hsu, W. Paul and K. Binder, *Macromol. Theory Simul.*, 2011, **20**, 510–525.
18 H.-P. Hsu, W. Paul and K. Binder, *Macromolecules*, 2014, **47**, 427–437.
19 G. S. Grest and M. Murat, *Macromolecules*, 1993, **26**, 3108–3117.
20 J. Klein, D. Perahia and S. Warburg, *Nature*, 1991, **352**, 143–145.
21 U. Raviv, S. Giasson, N. Kampf, J.-F. Gohy, R. Jerome and J. Klein, *Nature*, 2003, **425**, 163–165.
22 J. Klein, E. Kumacheva, D. Mahalu, D. Perahia and L. J. Fetters, *Nature*, 1994, **370**, 634–636.
23 G. S. Grest, *Polymers in Confined Environments*, Springer Berlin Heidelberg, 1999, vol. 138, pp. 149–183.
24 U. Raviv and J. Klein, *Science*, 2002, **297**, 1540–1543.
25 J. Seror, Y. Merkher, N. Kampf, L. Collinson, A. J. Day, A. Maroudas and J. Klein, *Biomacromolecules*, 2011, **12**, 3432–3443.
26 J. Seror, Y. Merkher, N. Kampf, L. Collinson, A. J. Day, A. Maroudas and J. Klein, *Biomacromolecules*, 2012, **13**, 3823–3832.
27 C. Kiani, L. Chen, Y. J. Wu, A. J. Yee and B. B. Yang, *Cell Res.*, 2002, **12**, 19–32.
28 J. Klein, *Polym. Adv. Technol.*, 2012, **23**, 729–735.
29 R. Beck, J. Deek and C. R. Safinya, *Biochem. Soc. Trans.*, 2012, **40**, 1027–1031.
30 R. Beck, J. Deek, J. B. Jones and C. R. Safinya, *Nat. Mater.*, 2009, **9**, 40–46.
31 P. A. Janmey, J.-F. Leterrier and H. Herrmann, *Curr. Opin. Colloid Interface Sci.*, 2003, **8**, 40–47.
32 S. Kumar, X. Yin, B. D. Trapp, J. H. Hoh and M. E. Paulaitis, *Biophys. J.*, 2002, **82**, 2360–2372.
33 A. Laser-Azogui, M. Kornreich, E. Malka-Gibor and R. Beck, *Current Opinion in Cell Biology*, 2015, **32**, 92 – 101.
34 I. M. Storm, M. Kornreich, A. Hernandez-Garcia, I. K. Voets, R. Beck, M. A. Cohen Stuart, F. A. M. Leermakers and R. de Vries, *J. Phys. Chem. B.*, 2015, **119**, 4084–4092.
35 A. Hernandez-Garcia, M. W. T. Werten, M. M. A. Cohen Stuart, F. A. de Wolf and R. de Vries, *Small*, 2012, **8**, 3491–3501.
36 M. W. T. Werten, W. H. Wisselink, T. J. Jansen-van den Bosch, E. C. de Bruin and F. A. de Wolf, *Protein Eng.*, 2001, **14**, 447–454.
37 G. H. Fredrickson, *Macromolecules*, 1993, **26**, 2825–2831.
38 Y. Rouault and O. V. Borisov, *Macromolecules*, 1996, **29**, 2605–2611.
39 Y. Tsukahara, Y. Ohta and K. Senoo, *Polymer*, 1995, **36**, 3413 – 3416.
40 Y. Nakamura, M. Koori, Y. Li and T. Norisuye, *Polymer*, 2008, **49**, 4877 – 4881.
41 X. Li, H. ShamsiJazeyi, S. L. Pesek, A. Agrawal, B. Hammouda and R. Verduzco, *Soft Matter*, 2014, **10**, 2008–2015.
42 S. T. Milner, T. A. Witten and M. E. Cates, *Macromolecules*, 1988, **21**, 2610–2619.
43 S. M. Balko, T. Kreer, P. J. Costanzo, T. E. Patten, A. Johner, T. L. Kuhl and C. M. Marques, *PLoS ONE*, 2013, **8**, e58392.
44 T. Kreer and S. M. Balko, *ACS Macro Lett.*, 2013, **2**, 944–947.
45 A. Milchev and K. Binder, *Soft Matter*, 2014, **10**, 3783–3797.
46 V. A. Parsegian, R. P. Rand, N. L. Fuller and D. C. Rau, *Meth. Enzymol.*, 1986, **127**, 400–416.
47 V. A. Parsegian, R. P. Rand and D. C. Rau, *Meth. Enzymol.*, 1995, **259**, 43–94.
48 O. Borisov, T. Birshtein and Y. Zhulina, *Polymer Science U.S.S.R.*, 1987, **29**, 1552 – 1559.
49 S. Bolisetty, S. Rosenfeldt, C. N. Rochette, L. Harnau, P. Lindner, Y. Xu, A. H. E. Müller and M. Ballauff, *Colloid and Polymer Science*, 2008, **287**, 129–138.

50 S. Rathgeber, T. Pakula, A. Wilk, K. Matyjaszewski, H. il Lee and K. L. Beers, *Polymer*, 2006, **47**, 7318 – 7327.

51 H. Benoit, *Comptes Rendus*, 1957, pp. 2244–2247.

52 B. Hammouda, *Adv. Polym. Sci.*, 1993, **106**, 87–133.

53 A. Guinier and G. Fournet, *Small-Angle Scattering of X-Rays*, John Wiley and Sons, New York, 1955.

54 J. S. Pedersen, *Advances in Colloid and Interface Science*, 1997, **70**, 171 – 210.

55 G. J. Fleer, M. A. Cohen Stuart, J. M. H. M. Scheutjens, T. Cosgrove and B. Vincent, *Polymers at interfaces*, Chapman and Hall, London, 1993.

56 C. M. Wijmans, F. A. M. Leermakers and G. J. Fleer, *Langmuir*, 1994, **10**, 4514–4516.

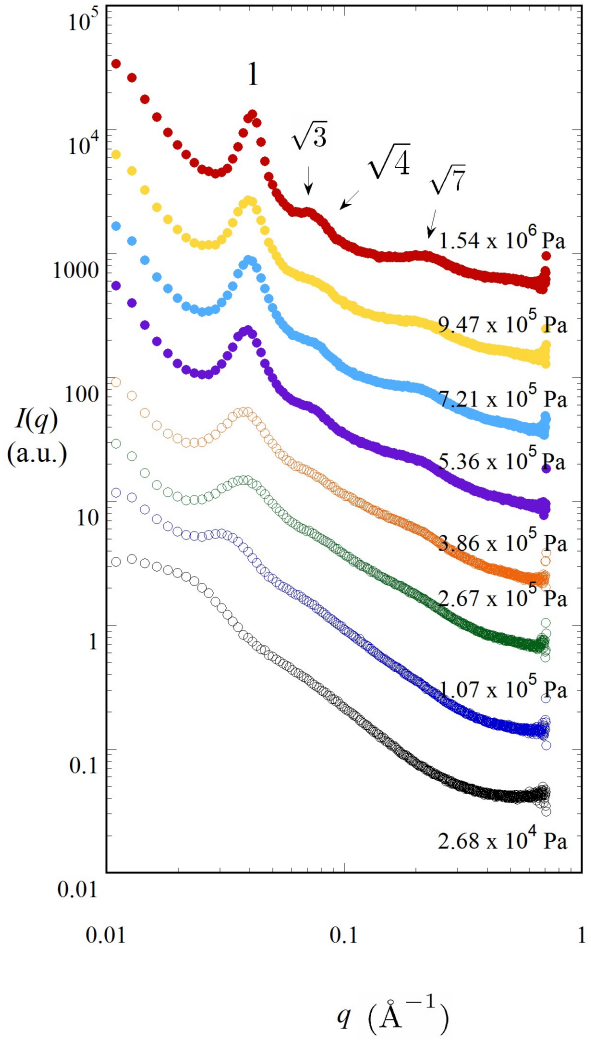

Fig. 4 Small angle X-ray scattering (SAXS) profiles of scattering intensity vs. magnitude of the wavevector (log I vs. log q) for DNA-bottlebrushes with a protein to DNA ratio of $\Gamma = 10$. The samples were equilibrated against PEG solutions of: 30 (red), 25 (yellow), 22.5 (light blue), 20 (purple), 17.5 (orange), 15 (green), 10 (dark blue), 5 wt%(black). Open symbols represent isotropic samples and closed symbols are birefringent samples. The curves have been shifted vertically for clarity.

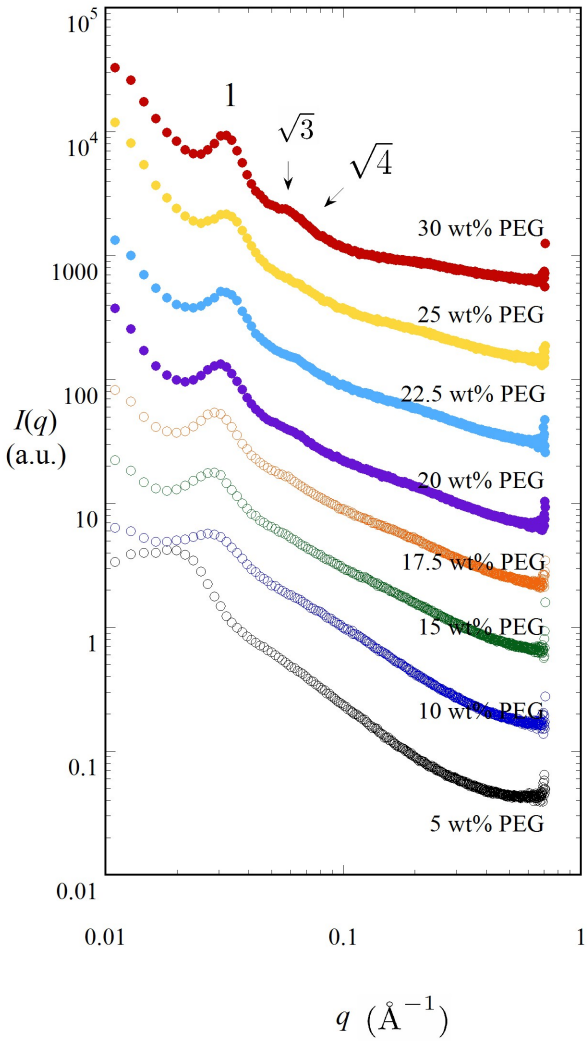

Fig. 5 Small angle X-ray scattering (SAXS) profiles of scattering intensity vs. magnitude of the wavevector (log I vs. log q) for DNA-bottlebrushes with a protein to DNA ratio of Γ = 30. The samples were equilibrated against PEG solutions of: 30 (red), 25 (yellow), 22.5 (light blue), 20 (purple), 17.5 (orange), 15 (green), 10 (dark blue), 5 wt%(black). Open symbols represent isotropic samples and closed symbols are birefringent samples. The curves have been shifted vertically for clarity.

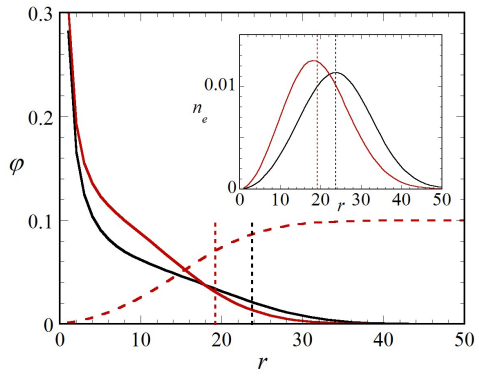

Fig. 6 Radial volume fraction profile $\varphi(r)$ for the default case $h = 4$ and side chains $N = 400$ for marginal solvent conditions $\chi = 0.4$ in the absence of free polymer (black curve) and in the presence of free polymers (red curve). The free polymers are $N = 400$ segments long with a bulk volume fraction of $\varphi^b = 0.1$ (dashed profile). In the inset we give the number distribution $n(r)$ of the free ends of the grafted chains, both in the presence (red) and in the absence (black) of free polymer. The vertical dotted lines represent the mean position of the end-points which is a measure for the thickness of the brush D (in lattice units).

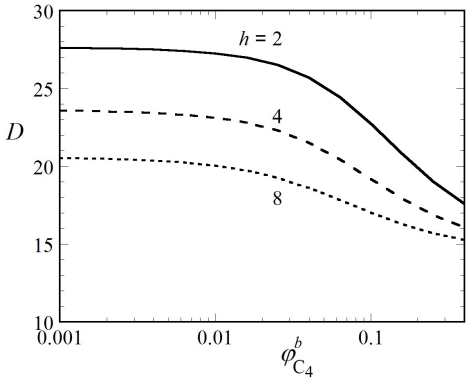

Fig. 7 The brush height (D) in lattice units b as a function of the volume fraction φ^b of freely dispersed C_4 (400 segments long) chains for three values of the grafting distance $h = 2,\ 4,\ 8$.

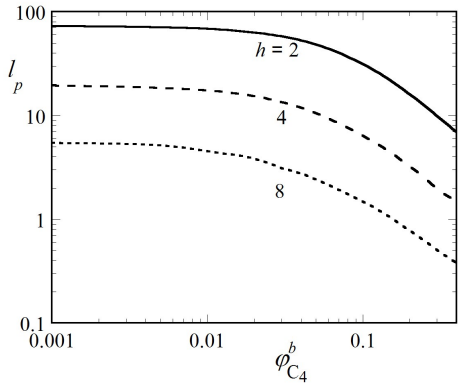

Fig. 8 Induced persistence length (l_p) of the bottlebrush as a function of bulk volume fractions φ^b of the freely dispersed C_4 polymers for three values of the grafting density (i.e. distance between grafts $h = 2,\ 4,\ 8$) in double logarithmic coordinates.

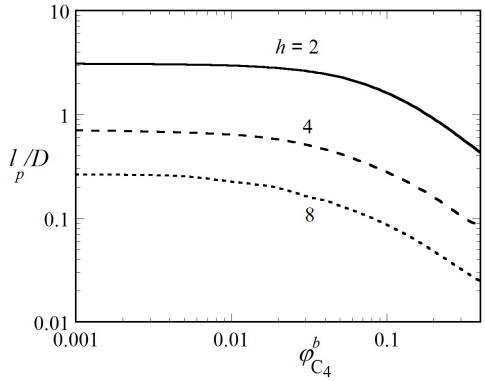

Fig. 10 SCF predictions for the aspect ratio (l_p/D) as a function of the volume fractions φ^b of C_4 for three values of the grafting density (distance between grafts $h = 2,\ 4,\ 8$). These results are found by combination of results of Figure 8 and 7.

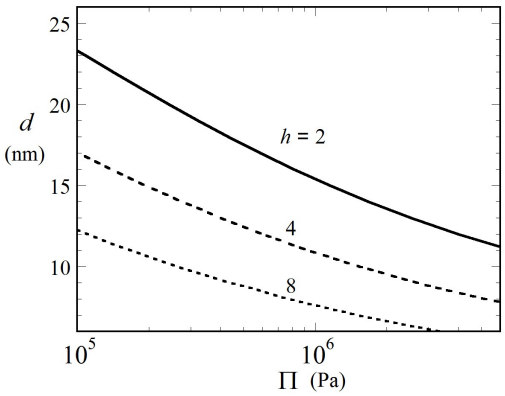

Fig. 9 SCF predictions for the distances (d) between bottlebrushes as a function of osmotic pressure Π (Pa) computed within a "cell model" for three values of the distance between the grafted chains $h = 2,\ 4,\ 8$ in the absence of free polymer.

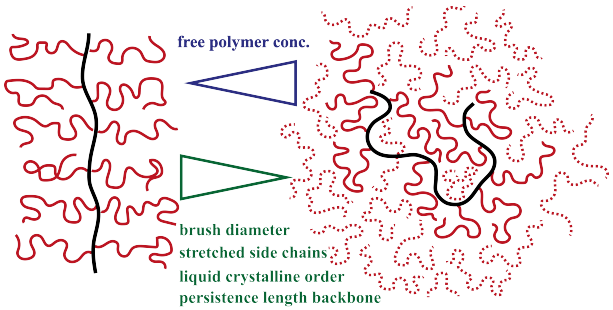

TOC figure: Increasing free polymer conc. inhibits liquid crystalline ordering of supramolecular bottlebrushes due to a loss in the stretching of the side chains.